

Fermi level depinning and contact resistivity reduction using a reduced titania interlayer in n-silicon metal-insulator-semiconductor ohmic contacts

Ashish Agrawal, Joyce Lin, Michael Barth, Ryan White, Bo Zheng, Saurabh Chopra, Shashank Gupta, Ke Wang, Jerry Gelatos, Suzanne E. Mohny, and Suman Datta

Citation: *Applied Physics Letters* **104**, 112101 (2014); doi: 10.1063/1.4868302

View online: <http://dx.doi.org/10.1063/1.4868302>

View Table of Contents: <http://scitation.aip.org/content/aip/journal/apl/104/11?ver=pdfcov>

Published by the [AIP Publishing](#)

Articles you may be interested in

Fermi-level depinning and contact resistance reduction in metal/n-Ge junctions by insertion of W-encapsulating Si cluster films

Appl. Phys. Lett. **104**, 062105 (2014); 10.1063/1.4864321

Contact resistivity reduction through interfacial layer doping in metal-interfacial layer-semiconductor contacts

J. Appl. Phys. **113**, 234505 (2013); 10.1063/1.4811340

A unified model for insulator selection to form ultra-low resistivity metal-insulator-semiconductor contacts to n-Si, n-Ge, and n-InGaAs

Appl. Phys. Lett. **101**, 042108 (2012); 10.1063/1.4739784

Low resistance Ti Ohmic contacts to 4H-SiC by reducing barrier heights without high temperature annealing

Appl. Phys. Lett. **100**, 263503 (2012); 10.1063/1.4730435

Fermi level depinning in metal/Ge Schottky junction for metal source/drain Ge metal-oxide-semiconductor field-effect-transistor application

J. Appl. Phys. **105**, 023702 (2009); 10.1063/1.3065990



Re-register for Table of Content Alerts

Create a profile.



Sign up today!



Fermi level depinning and contact resistivity reduction using a reduced titania interlayer in n-silicon metal-insulator-semiconductor ohmic contacts

Ashish Agrawal,¹ Joyce Lin,² Michael Barth,¹ Ryan White,³ Bo Zheng,⁴ Saurabh Chopra,⁴ Shashank Gupta,⁴ Ke Wang,¹ Jerry Gelatos,⁴ Suzanne E. Mohny,² and Suman Datta¹

¹Department of Electrical Engineering, The Pennsylvania State University, University Park, Pennsylvania 16802, USA

²Department of Material Science and Engineering, The Pennsylvania State University, University Park, Pennsylvania 16802, USA

³North Carolina State University, Raleigh, North Carolina 27607, USA

⁴Applied Materials, Santa Clara, California 95054, USA

(Received 18 January 2014; accepted 19 February 2014; published online 17 March 2014)

Experimental evidence of reduction of ultrathin TiO₂ by Ti is presented and its effect on Fermi level depinning and contact resistivity reduction to Si is experimentally studied. A low effective barrier height of 0.15 V was measured with a Ti/10 Å TiO_{2-x}/n-Si MIS device, indicating 55% reduction compared to a metal/n-Si control contact. Ultra-low contact resistivity of $9.1 \times 10^{-9} \Omega\text{-cm}^2$ was obtained using Ti/10 Å TiO_{2-x}/n+ Si, which is a dramatic 13X reduction from conventional unannealed contacts on heavily doped Si. Transport through the MIS device incorporating the effect of barrier height reduction and insulator conductivity as a function of insulator thickness is comprehensively analyzed and correlated with change in contact resistivity. Low effective barrier height, high substrate doping, and high conductivity interfacial layer are identified as key requirements to obtain low contact resistivity using MIS contacts. © 2014 AIP Publishing LLC. [<http://dx.doi.org/10.1063/1.4868302>]

External parasitic resistance (R_{EXT}) is a major problem for continued MOSFET scaling. According to International Technology Roadmap for Semiconductors (ITRS), R_{EXT} will significantly degrade device performance unless parasitic metal-semiconductor (M-S) contact resistance (ρ_C) is decreased to the sub- $10^{-8} \Omega\text{-cm}^2$ regime.¹ A key metric of a M-S contact is the Schottky barrier height (Φ_{Bn}) predicted by the Schottky-Mott rule to be the difference in the metal workfunction and semiconductor electron affinity.² However, the observed Φ_{Bn} differs significantly from the calculated value, which is usually attributed to metal-induced gap states (MIGS) or defects.

The approach for addressing this problem can be understood by looking at the dependencies of ρ_C , which is given by

$$\rho_C \propto \exp \left[\frac{4\pi\sqrt{\epsilon \times m^*} \Phi_{Bn}}{h \sqrt{N_D}} \right], \quad (1)$$

where ρ_C is the specific contact resistivity, ϵ is the semiconductor permittivity, N_D is the surface doping concentration, and m^* is the carrier effective mass.³ Due to solid solubility limit for dopants in Si, the only way to reduce ρ_C is through a reduction in Φ_{Bn} . State-of-the-art NiSi contacts have a Φ_{Bn} near midgap on Si due to Fermi level pinning, requiring advanced technologies or materials for barrier height reduction.

Recently, several groups have reported obtaining band-edge Φ_{Bn} by releasing the Fermi level pinning (FLP) of M-S contacts using a thin interfacial dielectric.⁴⁻⁶ The interfacial dielectric functions as a tunnel barrier to MIGS while being thin enough to allow significant conduction through it. In this way, the dielectric prevents occupation of MIGS at the

semiconductor interface by metal electrons, which allows the Φ_{Bn} to be dominated by Φ_M . The key transport mechanisms are schematically shown in Fig. 1(a). An interfacial oxide with a low conduction band offset and low tunneling effective mass is desirable for achieving low contact resistivity using MIS contacts. An insulator-silicon system with these characteristics results in lowering of the minimum achievable contact resistivity that can be obtained before the resistance of the insulator becomes the limiting factor (Fig. 1(b)). Analytical modeling of MIS contacts performed by simultaneously incorporating Fermi level unpinning and tunneling resistance as a function of insulator thickness indicated TiO₂ as an ideal interfacial layer to obtain sub- $10^{-8} \Omega\text{-cm}^2$ contact resistivity on n-Si.⁷

In this work, we present a comprehensive experimental study of Fermi level depinning, effective Φ_{Bn} reduction to Si and contact resistivity reduction using an ultrathin TiO₂ insulator between metal and Si. Experiments have been performed for different insulator thickness and metals on lightly doped silicon to study barrier height reduction and effective pinning for the MIS configuration. Next, the effect of the insulator on contact resistivity to n+ Si was analyzed using TiO₂ insulator MIS devices. Finally, the transport through MIS devices is analyzed by analytical modeling of various resistance components and dominant factors are enlisted.

An n-type phosphorus doped (100)-oriented Si wafer with $10^{15}/\text{cm}^3$ doping was used to fabricate Schottky diodes to extract the Schottky barrier height (SBH). Refined Transmission Line Method (RTLM) structures⁸ with varying gap spacing were fabricated on heavily doped Si with a doping concentration $4.1 \times 10^{20}/\text{cm}^3$ to extract contact resistivity. Samples were dipped in H₂SO₄:H₂O₂ = 100:1 for 20 min followed by dilute HF solution (H₂O:HF = 10:1) for 2 min and

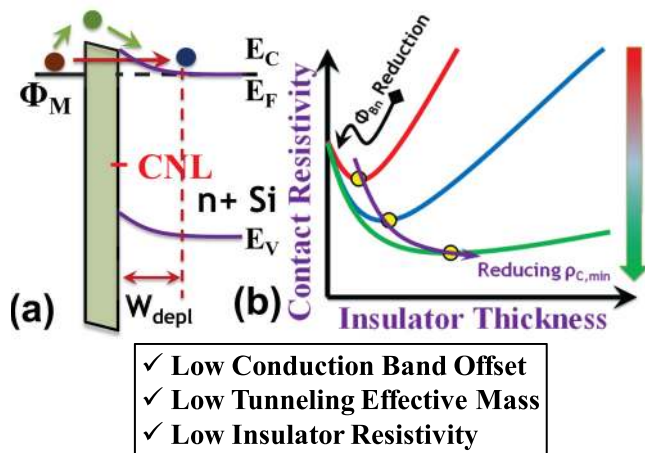


FIG. 1. (a) Schematic band diagram of the MIS contact structure with low conduction band offset for electrons highlighting tunneling and thermionic emission as dominant transport mechanisms (b) schematic contact resistivity vs. insulator thickness indicating reduced minimum achievable contact resistivity for low band offset, low tunneling effective mass and low insulator resistivity.

rinsed in de-ionized water. Next, the samples were immediately loaded in a Cambridge Savannah atomic layer deposition (ALD) system to deposit thin TiO_2 layer with thicknesses of 10 Å and 20 Å. Further, four metals (Ni, Pt, Ti, and Mo) with 20 nm thickness capped with 80 nm Au were deposited by e-beam evaporation system to study the effect of metal workfunction on MIS contacts. Finally, the contact metal was patterned by a lift-off process. Fig. 2 shows the XPS data for 20 Å, as-deposited ALD TiO_2 on Si before metal deposition. The binding energy location of Ti^{4+} and O^{2-} peaks indicate stoichiometric TiO_2 on Si deposited using ALD. A weak signal in O 1s spectrum at 532 eV indicates the presence of hydroxides probably from exposure to ambient.

The current-voltage (I-V) characteristics of Ni/ TiO_2 /n-Si MIS devices were measured as a function of varying TiO_2 thickness. Figure 3(a) shows the measured I-V characteristics of these devices at room temperature. Non-linear, rectifying behavior was observed for all the devices indicating thermionic emission dominated transport over the barrier. Without TiO_2 (0 Å curve), low reverse saturation current density was

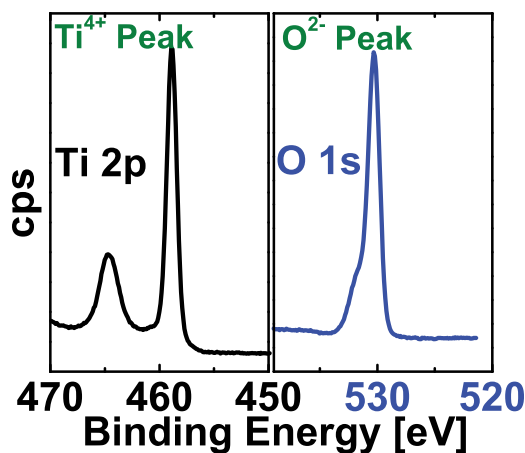


FIG. 2. XPS data showing Ti 2p and O 1s scan of 10 Å TiO_2 deposited by ALD on Si before metal deposition. The energy location of the peak is indicative of stoichiometric TiO_2 .

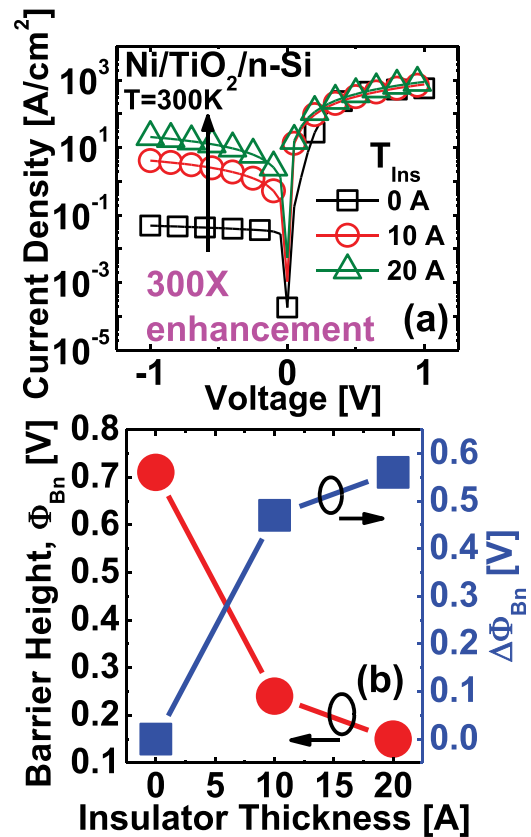


FIG. 3. (a) Experimental J-V characteristics of Ni/ TiO_2 /n-Si MIS devices at room temperature with increasing TiO_2 thickness showing 300× enhancement for 20 Å T_{ins} compared to the Ni/n-Si device, indicative of effective barrier height reduction. (b) extracted effective barrier height using I-V-T measurements on Ni/ TiO_2 /n-Si MIS devices with increasing T_{ins} indicate reduction of barrier height.

observed as expected due to large, pinned Φ_{Bn} between Ni and silicon. As the TiO_2 thickness was increased to 10 Å and 20 Å, a significant increase (300×) in reverse current density was observed. This is evidence of reduction in effective Φ_{Bn} , which increases thermionic emission, and hence the reverse saturation current. The forward bias current density shows negligible change with TiO_2 thickness, indicating series resistance limited current due to low substrate doping. Increase in reverse saturation current density with increasing TiO_2 thickness indicated effective Φ_{Bn} reduction resulting from reduced MIGS occupation in the silicon bandgap and hence Fermi level depinning.

Temperature dependent I-V measurements were performed between 300 K and 375 K for 0 Å, 10 Å, and 20 Å TiO_2 MIS devices to extract the effective Φ_{Bn} . The Richardson plot of $\ln(J_0/T^2)$ versus $1000/T$ was analyzed, where J_0 is the reverse saturation current and T is the temperature. The slope of such a plot is $-q\Phi_{Bn}/k$, where q is charge and k is the Boltzmann constant.⁹ The extracted Φ_{Bn} (Fig. 3(b)) was 0.72 V for Ni/n-Si M-S contact indicating pinning at Si midgap, reduced Φ_{Bn} of 0.24 V for 10 Å TiO_2 and 0.15 V for 20 Å TiO_2 MIS devices. This is a substantial 55% reduction in barrier height from the 0 Å case. The reduction in effective Φ_{Bn} for thicker TiO_2 explains increasing reverse saturation current density for the 10 Å and 20 Å TiO_2 MIS contacts.

With the introduction of the TiO_2 interlayer, the Fermi-level unpins from the Si charge neutrality level (CNL)

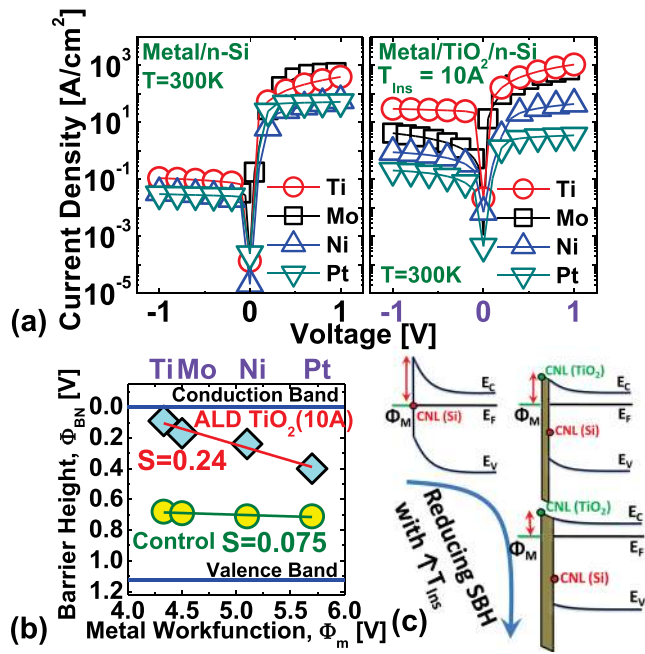


FIG. 4. (a) Experimental J-V characteristics of metal/n-Si and metal/10 Å TiO₂/n-Si with Ti, Mo, Ni, and Pt as metals showing larger change in reverse saturation current density with changing metal workfunction for MIS devices compared to the M-S case. Additionally higher reverse saturation current indicates lower effective barrier height, (b) experimentally extracted effective barrier height by I-V-T measurements on metal/n-Si and metal/10 Å TiO₂/n-Si devices showing higher S factor and reduced barrier height for MIS devices, (c) schematic showing shifting of Fermi level pinning from the Si CNL to the TiO₂ CNL with increasing T_{ins}.

but pins to the TiO₂ CNL due to occupation of MIGS at the TiO₂ surface by metal electrons. MIS contacts with 10 Å TiO₂ using metals with varying metal workfunction like Ti, Mo, Ni, and Pt were fabricated to understand the effective pinning factor, S, for the MIS contact scheme and to compare with metal/Si devices. In Fig. 4(a), measured I-V characteristics of metal/n-Si and metal/(10 Å) TiO₂/n-Si devices are shown. Without TiO₂, negligible change in the reverse current density is observed with varying metal workfunction. For the 10 Å TiO₂ MIS contact, higher reverse current density in addition to higher modulation with varying metal workfunction is obtained indicating larger change in Φ_{Bn} with Φ_m . I-V-T measurements were performed for M-S and MIS devices with 10 Å TiO₂ with each metal to extract effective Φ_{Bn} . Fig. 4(b) shows the extracted Φ_{Bn} vs. Φ_m for 0 Å TiO₂ and 10 Å TiO₂ MIS contacts with different metals. Low effective Φ_{Bn} of 0.15 V was obtained with Ti and 10 Å TiO₂ insulator, which is a significant 76% reduction compared to the Ti/n-Si device. The pinning factor, S, extracted from the slope of Φ_{Bn} vs. Φ_m was obtained as 0.075 for metal/n-Si and 0.24 for metal/10 Å TiO₂/n-Si. The implication that the Fermi level is pinned at the metal-Si interface is as expected. The deviation of S factor from Schottky limit (S = 1) for the metal/TiO₂/Si MIS contacts indicates that the Fermi level is pinned at the metal-TiO₂ interface with the CNL being located close to the conduction band edge (Fig. 4(c)).

To understand the effect of Fermi-level depinning and reduced effective Φ_{Bn} on contact resistivity on n+ Si, TLM measurements were performed with 0 Å, 10 Å, and 20 Å TiO₂

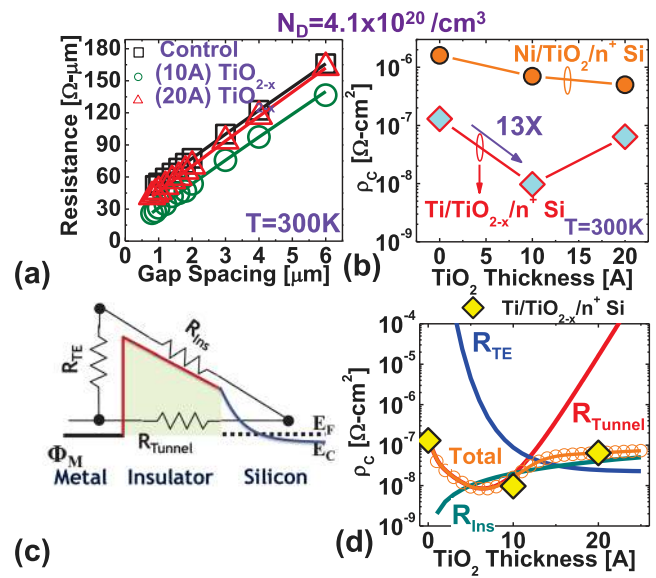


FIG. 5. (a) Resistance vs. TLM gap spacing data for the Ti/n+ Si and Ti/TiO₂/n+ Si MIS devices with T_{ins} = 10 Å and 20 Å on $4.1 \times 10^{20} / \text{cm}^3$ doped Si, (b) extracted contact resistivity vs. TiO₂ thickness with Ni and Ti as metals on heavily doped Si, (c) schematic of MIS contact highlighting tunnel resistance R_{Tunnel}, resistance associated with thermionic emission R_{TE} and insulator resistivity R_{ins} as contributors to total contact resistivity, (d) experimental (diamond symbols) and modeled contact resistivity vs. insulator thickness indicating different components. For small T_{ins}, R_{Tunnel} limits the ρ_c and for thick T_{ins}, insulator resistivity limits the ρ_c .

interlayer on $4.1 \times 10^{20} / \text{cm}^3$ doped silicon. Ti was selected as the metal due to low effective barrier height as extracted on n-Si with TiO₂. Fig. 5(a) shows measured resistance as a function of TLM gap spacing for 0 Å, 10 Å, and 20 Å TiO₂ thickness with Ti metal and was used to extract contact resistivity, ρ_c . Fig. 5(b) shows the ρ_c measured using 4-point TLM measurements as a function of TiO₂ thickness on n+ Si with Ni and Ti metals. Without any insulator, $\rho_c = 1.8 \times 10^{-6} \Omega\cdot\text{cm}^2$ for Ni/Si, and a 10X smaller $\rho_c = 1.4 \times 10^{-7} \Omega\cdot\text{cm}^2$ for Ti/Si was obtained, which is similar to results reported for an unannealed contact.¹⁰ With the Ni/TiO₂/Si MIS contact, ρ_c reduction was observed with a minimum ρ_c of $5 \times 10^{-7} \Omega\cdot\text{cm}^2$ for 20 Å TiO₂, commensurate with Φ_{Bn} reduction with increasing T_{ins}. A dramatic 13X reduction in ρ_c was obtained with Ti metal and a 10 Å TiO₂ MIS contact, with ρ_c of $9.1 \times 10^{-9} \Omega\cdot\text{cm}^2$. For thicker 20 Å TiO₂; however, ρ_c increased again by 10X to $9 \times 10^{-8} \Omega\cdot\text{cm}^2$. This trend in ρ_c in conjunction with experiments on lightly doped Si MIS devices demanded further investigation of transport through the MIS contact. Hence, analytical modeling of electron transport in the MIS device was performed.

The total resistivity of MIS contact was divided into the contribution from R_{Tunnel}, the tunneling resistance of TiO₂ insulator in parallel with R_{TE}, resistance associated with over the barrier thermionic emission of electrons from the metal in TiO₂ in series with R_{ins}, the resistance offered due to scattering of electrons emitted after thermionic emission in TiO₂ (Fig. 5(c)). The result of this modeling as a function of insulator thickness is shown in Fig. 5(d). Fermi level depinning with increasing T_{ins} exponentially reduces R_{TE} due to reduction in effective Φ_{Bn} . R_{Tunnel} reduces due to the reduction in

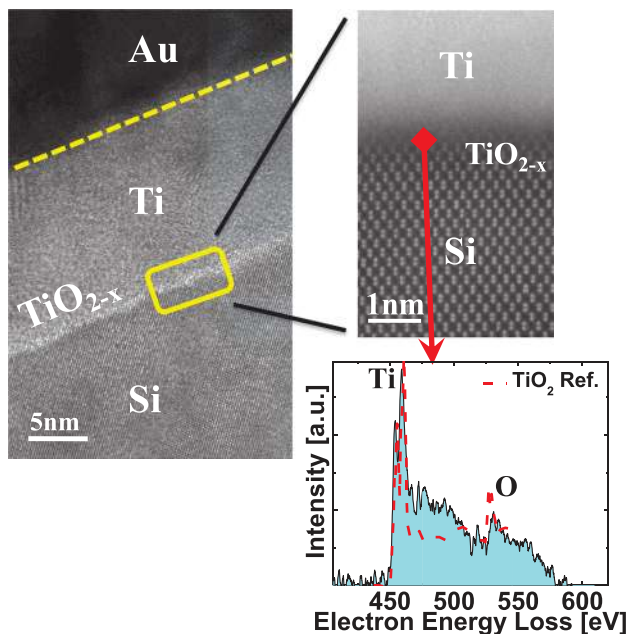


FIG. 6. Cross-sectional TEM image of a Ti/TiO_{2-x}/Si MIS contact showing an ultrathin amorphous, uniform TiO_{2-x} insulator. EELS point scan at the interfacial layer between Ti and Si suggests reduced oxygen content in the TiO₂ compared to a stoichiometric TiO₂ (red dashed line).

tunneling barrier height, however, increases for large T_{Ins} due to increasing tunneling distance. Fig. 6 shows the cross section TEM of the Ti/TiO₂/Si MIS contact. An EELS scan performed at the interface of TiO₂ and silicon reveals a significantly reduced oxygen intensity compared to stoichiometric TiO₂ for the same areal intensity of Ti.¹¹ This indicates that an oxygen deficient TiO_{2-x} is present at the interface due to oxygen gettering by Ti metal, which is known to be more conductive than stoichiometric TiO₂.¹² R_{Ins} was calculated using a significantly reduced TiO_{2-x} resistivity of 10 $\Omega\text{-cm}$ as obtained by 4-point conductivity measurements of ultrathin TiO_{2-x} deposited on an insulating substrate. The contact resistivity reduction for 10 Å TiO_{2-x} is due to reduction in effective Φ_{Bn} , whereas, with thicker insulator thickness of 20 Å, ρ_C is limited by series resistance due to scattering of electrons in TiO_{2-x}. Hence, to obtain low contact resistivity using MIS contacts, it is advantageous to choose an interfacial layer with low band offset in addition to higher conductivity.

In summary, effective barrier height reduction has been experimentally studied and demonstrated on n-Si using MIS contacts with reduced ALD TiO₂ interlayers. Low effective Φ_{Bn} of 0.15 V was obtained using temperature-dependent measurements of the Ti/10 Å TiO₂/n-Si MIS contact which is 55% lower than the Ti/n-Si M-S contact, making it an excellent candidate to obtain low contact resistivity using MIS devices. TLM measurements performed with the TiO₂ interlayer on n+ Si indicated a low contact resistivity of $9.1 \times 10^{-9} \Omega\text{-cm}^2$ for 10 Å TiO₂, which represents a 13 \times reduction compared to Ti/n+ Si contacts. In-depth modeling of transport through MIS contacts was performed by evaluating the contribution from tunneling resistance, thermionic emission, and series resistance from the TiO₂ interlayer. The reduction in ρ_C is attributed to reduction in effective Φ_{Bn} due to the pinning at the metal/TiO₂ interface, and the subsequent increase in ρ_C at high T_{Ins} is due to series resistance of the TiO₂ insulator. Reduction of interfacial layer resistivity using oxygen-deficient TiO_{2-x} is key for obtaining low ρ_C in addition to low barrier height and high substrate doping.

This publication was supported by the Pennsylvania State University Materials Research Institute Materials Characterization and Nanofabrication Laboratories and the National Science Foundation Cooperative Agreement No. ECS-0335765.

¹"The International Technology Roadmap for Semiconductors (ITRS), <http://www.itrs.net/>," Technical Report, 2011.

²R. T. Tung, *Mater. Sci. Eng.* **35**, 1 (2001).

³A. Yu, *Solid-State Electron.* **13**, 239 (1970).

⁴D. Connelly, C. Faulkner, D. Grupp, and J. Harris, *IEEE Trans. Nanotechnol.* **3**, 98 (2004).

⁵M. Kobayashi, A. Kinoshita, K. Saraswat, H.-S. Wong, and Y. Nishi, *Symp. VLSI Technol., Dig. Tech. Pap.* **2008**, 54–55.

⁶A. Agrawal, J. Lin, B. Zheng, S. Sharma, S. Chopra, K. Wang, A. Gelatos, S. Mohny, and S. Datta, *Symp. VLSI Technol., Dig. Tech. Pap.* **2013**, T200–T201.

⁷A. Agrawal, N. Shukla, K. Ahmed, and S. Datta, *Appl. Phys. Lett.* **101**, 042108 (2012).

⁸R. Dormaier, S. E. Mohny, and J. Vac. *Sci. Technol., B: Microelectron. Nanometer Struct.* **30**, 031209 (2012).

⁹J. -Y. J. Lin, A. M. Roy, A. Nainani, Y. Sun, and K. C. Saraswat, *Appl. Phys. Lett.* **98**, 092113 (2011).

¹⁰P. Revva, A. Kastanas, and A. Nassiopoulou, *J. Electrochem. Soc.* **144**, 4072 (1997).

¹¹C.-N. Huang, J.-S. Bow, Y. Zheng, S.-Y. Chen, N. Ho, and P. Shen, *Nanoscale Res. Lett.* **5**, 972 (2010).

¹²K. Zakrzewska, *Adv. Mater. Sci. Eng.* **98**, 0987 (2012).